J. Appl. Cryst. (1998). **31**, 128–135

On the Analysis of Reversible Light-Induced Changes in Molecular Crystals

Y. Ozawa,† M. R. Pressprich and P. Coppens*

Department of Chemistry, Natural Sciences Complex, State University of New York at Buffalo, Buffalo, New York 14260-3000, USA. E-mail: coppens@acsu.buffalo.edu

(*Received 24 December 1996; accepted 23 May 1997*)

Abstract

New photocrystallographic and cryogenic techniques are tested in a 40 K study of the 2.44 ms lifetime excited state of [$RhBr_2$(pyridine-d_5)]Br. A modulation method is used in which a laser beam is interrupted by a mechanical chopper with a preselected frequency and the diffracted X-ray beam gated in synchronization with the chopper phase. Wilson-type plots of the response ratio η, defined as $\eta_{hkl} = [I_{on}(hkl) - I_{off}(hkl)]/I_{off}(hkl)$, give evidence of a small ($\simeq$ 2 K) temperature increase upon laser irradiation of the crystal at 40 K. The temperature change decreases when the chopper frequency is increased from 20 to 40 to 80 Hz, pointing to a gradual temperature increase during the laser-on period. A least-squares method for the refinement of excited-state parameters, with the experimental response ratios as observations, is described and applied using 46 experimental values of η. Although there is an indication that the Rh–Br bonds are shortened on excitation, the current data-set is too limited to allow unequivocal determination of the geometry changes upon excitation; the study presented is therefore primarily a description of the development and testing of new techniques.

1. Introduction

The periodic time structure of synchrotron radiation is opening up a new field of crystallographic research, in which chemical changes induced by pulsed external perturbations are monitored at the atomic level on very short timescales. Of particular interest is the effect of laser excitation on molecular crystals and semiconductors. The possibility of studying the geometry and eventually the electron density of excited states during electron-transfer processes is one of the ultimate goals of photocrystallography, and is expected to have widespread relevance.

The study of such generally reversible processes in crystals requires special instrumentation and data acquisition and processing algorithms. Using a rotating-anode source, we have previously studied the response of crystals to pulsed external electric fields with a modulation method (Graafsma, Paturle *et al.*, 1992; Graafsma, Coppens *et al.*, 1993; Paturle *et al.*, 1991) and have developed equipment for the study of light-irradiated crystals (White *et al.*, 1994). In general, upon irradiation of a molecular crystal with the appropriate wavelength, only a fraction of the molecules will be excited. When the laser light is periodically interrupted by a chopper, a steady-state concentration of excited molecules will be established in the crystal during each light-on period. As shown below, this concentration is proportional to the lifetime of the excited species. Therefore, the chopper method is only suitable for the study of excitations with lifetimes down to about 1 ms. It is used here principally to obtain experience for planned studies of shorter-lived species, to be based on nonequilibrium methods.

We describe details of the equipment used and give expressions appropriate for the refinement of a partially excited crystal. The methods are applied to a small rotating-anode data-set on a Rh coordination complex.

2. Experimental

2.1. *Apparatus*

The apparatus used has three components: (i) the chopper control and gating signal generator electronics; (ii) the counting digital I/O board; and (iii) the laser optics. The apparatus is controlled by a modified version of the program *ZACK* (Restori, 1989) and is a C^{++} program on a 486 IBM-compatible PC.

2.1.1. *Chopper controller.* A diagram of the instrumentation is given in Fig. 1, while the timing sequence is illustrated in Fig. 2. The laser light is chopped by a disk with 10 or 30 slots, attached to a stepping motor. The chopping rate is controlled within the range 5–180 Hz with the chopper controller. An infrared diode sensor on the chopper wheel produces a light-on and light-off reference signal. The chopper controller, in which an 8 bit CPU (model Z8 Zilog) is installed, communicates with the host PC *via* serial I/O and sends laser 'on' and 'off' gating signals to the digital I/O board. The timing of the laser pulses passed by the chopper is synchronized with the signal from the diode sensor by posi-

† Permanent address: Department of Materials Science, Himeji Institute of Technology, Harima Science Park City, Kamigori-cho, Hyogo 678-12, Japan.

© 1998 International Union of Crystallography
Printed in Great Britain – all rights reserved

tional alignment of the blade relative to the laser beam. Because of the beam size and threshold of the diode sensor, the reference signal has a longer laser-on period than the laser itself.

2.1.2. *Timing digital I/O board.* An NI-DAQ (National Instruments Data Acquisition) PC-TIO-10 timing I/O board with ten 16 bit counters is installed in the host PC. X-ray signals from the pulse height analyzer (PHA) are fed into two sets of two-each concatenated 16 bit counters (labeled '3&4' and '8&9' in Fig. 1) mounted on the board. Each counter is gated by the signals from the chopper controller using two coaxial cables. These signals also gate the other two counters (labeled '5' and '10') on the board, which count the internal clock signal (1 MHz) to produce accurate total laser 'on' and 'off' acquisition times. Another counter (labeled '6') is used for providing time passed during a step of the scan, which is returned to the chopper controller.

2.1.3. *Optics.* 488 nm laser light generated by a Spectro-Physics model Stabilite 2017-06S Ar^+ laser is focused with a quartz lens, modulated by the chopper, and passed through a 500 μm fiber optic cable. A quartz lens is mounted on Newport five-axis gimbals at the exit of the optical fiber. The optical bench is mounted in a ring opposite the ϕ table which is an integral part of a HUBER 511 goniometer, as described previously (White *et al.*, 1994). A glass fiber mounted at the crystal position is used to align the laser beam along the ϕ axis and focus it on the crystal position. The light is guided to a photo transistor through the glass fiber. After alignment of the optical system the glass fiber is

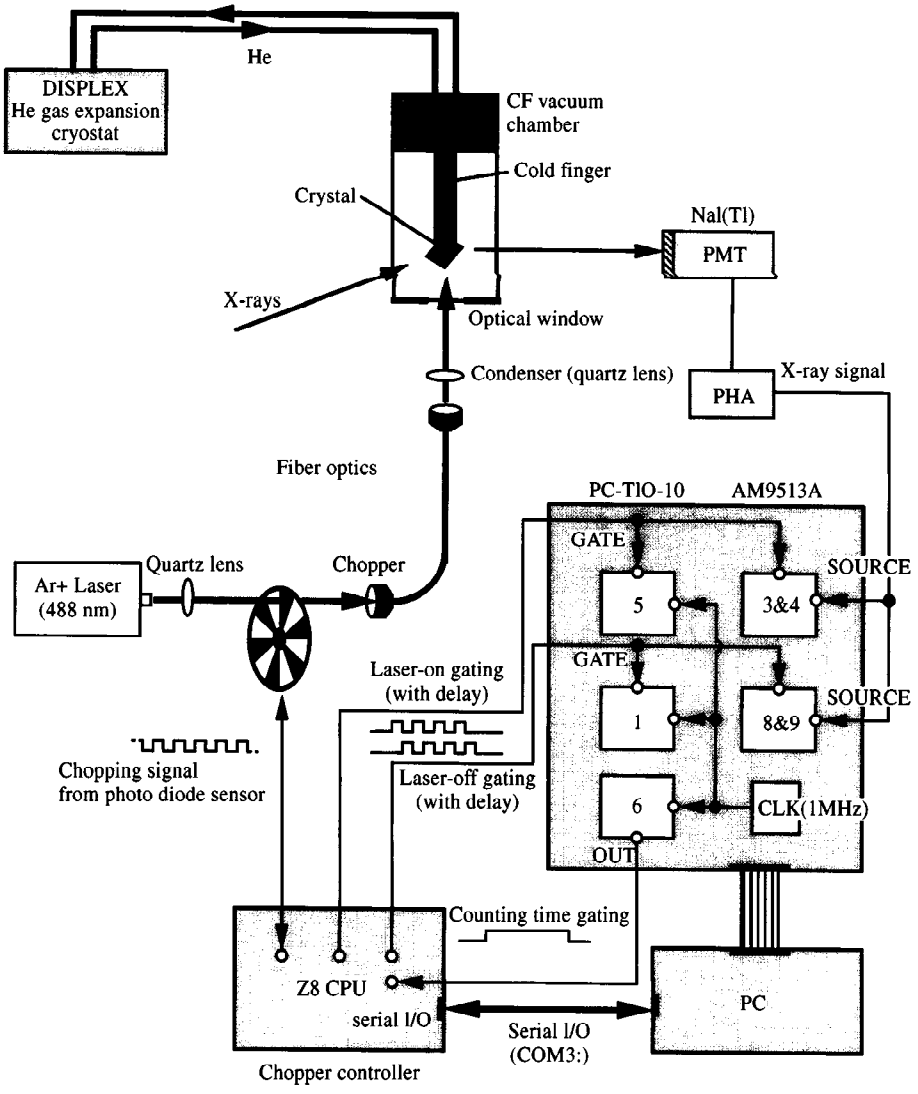

Fig. 1. Schematic of the experimental arrangement.

replaced by a crystal, mounted on an aluminium pin which is in thermal contact with the cryostat. The crystal and pin are enclosed in an Anholt Technologies XTRANS carbon fiber (CF) vacuum chamber, the roof of which is a quartz optical window to allow laser irradiation of the cold sample during the diffraction experiment.

2.2. *X-ray intensity measurement procedure*

The peak profiles were measured by step scanning. Because of the alternation of light-on and light-off periods, both light-on and light-off profiles can be collected in a single scan. This means that the resulting response ratios are not affected by long-term variations in intensity that may occur, due to, for example, slight crystal motion. The modulation method is therefore capable of measuring very small variations in intensity induced by the external perturbation.

Typically the scan of a reflection consists of 96 steps within a range of $\Delta\omega = 1.2°$, and 3 s acquisition time for each step, corresponding to a 5 min measurement time. The data collection procedure for each reflection is as follows: the *ZACK* software sends the information about chopping rate and delay time to the controller. When the controller responds that the chopper is ready, the goniometer moves to the starting angle and sends the acquisition gate signal to the chopper controller from the I/O board. The controller is providing the laser 'on' and 'off' gating signal during the acquisition time. The chopper always runs to keep the crystal at a thermal steady state. The laser 'on' and 'off' X-ray counts are normalized by using actual gating times. Typically 20 to 50 repeated scans are performed to achieve an accurate response ratio. X-ray counts for each step are accumulated, while the response ratio is evaluated in real time after each scan to check convergence.

2.3. *Population of the excited-state molecules*

We assume that the radiative and nonradiative decay processes involve only the triplet excited state and the singlet ground state. The time derivative of the number of excited molecules N^* under continuous laser illumination is given by

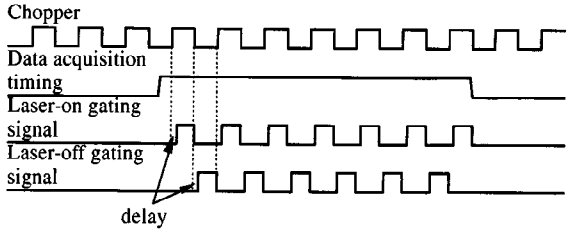

Fig. 2. The timing sequence of the experiment.

$$\frac{dN^*}{dt} = \frac{\phi_{isc}E}{h\nu} - \frac{N^*}{\tau_m}, \tag{1}$$

where ϕ_{isc} is the intersystem crossing yield from the singlet excited state to the triplet state, and τ_m the measured lifetime. E, the power of absorbed emission light, is a function of E_0, the power of the laser light beam (J s^{-1}), S_b is the area of the beam (mm^2), S_c the cross-sectional area of the crystal (mm^2), A the absorbance of the crystal (mm^{-1}), and L the crystal thickness (mm)

$$E = E_0 \frac{S_c}{S_b}(1 - 10^{-AL}). \tag{2}$$

The number of molecules in the triplet excited state is then obtained by integration as

$$N^* = E_0 \frac{S_c}{S_b}\frac{\phi_{isc}}{h\nu}\tau_m(1 - 10^{-AL})(1 - e^{-t/\tau_m}). \tag{3}$$

In the case that t is much longer than lifetime τ_m,

$$N^* = E_0 \frac{S_c}{S_b}\frac{\phi_{isc}}{h\nu}\tau_m(1 - 10^{-AL}). \tag{4}$$

As expected, the population of excited-state molecules is affected by both the absorbed energy and the lifetime of the triplet-state species. The absorbance of the crystal, A, is estimated from the absorbance of an aqueous solution of the complex, taking into account the relative concentrations.

To obtain the fractional conversion, the total number of molecules in the crystal is calculated from

$$N = ZV_{crystal}/U \tag{5}$$

where Z is the number of molecules in a unit cell, U the unit-cell volume, and V_{cryst} the volume of the crystal.

2.4. *Least-squares refinement over the response ratio*

A new structure refinement program *LASER*96 is used to refine the response ratios $\eta(hkl)$ obtained from the laser-modulated intensity measurement.

The response ratio is defined as the relative change in intensity, equal to the relative change in F^2, upon light irradiation

$$\eta_{hkl} = \frac{I_{on}(hkl) - I_{off}(hkl)}{I_{off}(hkl)} = \frac{F^2_{on}(hkl) - F^2_{off}(hkl)}{F^2_{off}(hkl)} = \frac{F^2_{on}(hkl)}{F^2_{off}(hkl)} - 1, \tag{6}$$

where F_{on} and F_{off} are the structure factors under light-on and light-off conditions, respectively. The derivatives of the response ratio towards a general parameter u can be written as

$$\begin{aligned}\frac{\partial\eta}{\partial u} &= \frac{\partial}{\partial u}\left(\frac{F_{on}^2}{F_{off}^2}\right) \\ &= 2\left(\frac{F_{on}}{F_{off}^2}\right)\frac{\partial F_{on}}{\partial u} \\ &= 2\left(\frac{1}{F_{off}^2}\right)\left(A_{on}\frac{\partial A_{on}}{\partial u} + B_{on}\frac{\partial B_{on}}{\partial u}\right),\end{aligned} \tag{7}$$

where A and B are real and imaginary parts of F, respectively.

The program allows refinement of the following excited-state parameters:

(*a*) The population p, describing the fraction of the excited molecules.

(*b*) A temperature scale factor k_B, to account for a temperature change during the laser-on period. A temperature scale factor has previously been used in the joint treatment of X-ray and neutron diffraction data (Coppens *et al.*, 1981). The concept is based on the assumption of proportionality of the temperature factor with the temperature itself and is valid in the classical limit. It is a reasonable approximation for the low-frequency modes dominant at the experimental temperature of $\simeq 40$ K (see, for example, Coppens, 1997). An alternative approach, based on an increase ΔB of an overall temperature B, lacks a theoretical basis.

(*c*) Positional and thermal parameters of the excited-state atoms, representing the geometry of the excited species.

(*d*) Rigid-body translational and rotational parameters for the ground-state species. The rigid-body motion allows for a possible change of the position and orientation of the ground-state molecules, which may occur as a result of the conversion to a multicomponent crystal. Such parameters were significantly different from zero for the partially excited crystals of nitrosyl complexes (Pressprich *et al.*, 1994; Fomitchev & Coppens, 1996; Carducci, Pressprich & Coppens, 1997). However, in the latter studies much larger excited-state concentrations were reached, as the lifetimes of the excited transition-metal nitrosyl species are essentially infinite at low temperatures.

For all parameters, with the exception of the population parameter p, we write, starting from (7)

$$\frac{\partial\eta}{\partial u} = \phi\frac{\partial F_{on}}{\partial u} = \phi\left[(1-p)\frac{\partial F_0}{\partial u} + p\frac{\partial F_1}{\partial u}\right], \tag{8}$$

introducing the symbol $\phi = 2F_{on}/F_{off}^2$, and using the relation $F_{on} = (1-p)F_0 + pF_1$, where F_0 and F_1 are the structure factors corresponding to the ground-state species in the partially excited crystal and the excited-state species, respectively. The structure factor F_0 may be different from the structure factor F_{off}, because of the rigid-body motions in response to the partial excitation. Relation (8) assumes that the excited-state species are randomly distributed over the crystal. A nonrandom distribution may lead to the appearance of superstructure reflections or broadening of the reflection profiles. In our studies of partially excited crystals of transition-metal nitrosyl complexes, no evidence was found for any ordering of the excited molecules, and a model based on a random distribution of the excited species refined smoothly in all cases (Pressprich *et al.*, 1994; Fomitchev & Coppens, 1996; Carducci, Pressprich & Coppens, 1997).

Only F_1 is dependent on the excited-state positional parameters x; thus

$$\frac{\partial\eta}{\partial x} = \phi p\frac{\partial F_1}{\partial x}. \tag{9}$$

The rigid-body displacement parameters R, on the other hand, only affect F_0:

$$\frac{\partial\eta}{\partial R} = \phi(1-p)\frac{\partial F_0}{\partial R}. \tag{10}$$

Both F_1 and F_0 are affected by a change in temperature. The derivative to the temperature scale factor k_B is given by

$$\frac{\partial\eta}{\partial k_B} = \phi\left[(1-p)\frac{\partial F_0}{\partial k_B} + p\frac{\partial F_1}{\partial k_B}\right] \tag{11}$$

with

$$\begin{aligned}\frac{\partial F_{0,1}}{\partial k_B} = -\sum_i \Big[f_i \exp 2\pi\mathbf{H}\cdot\mathbf{r}_i \sum_j\sum_k U_{ijk}h_jh_ka_j^*a_k^* \\ \times \exp(-k_BU_{ijk}h_jh_ka_j^*a_k^*)\Big].\end{aligned}$$

We note that the k_B derivative can be expressed as a sum of derivatives of the temperature factors

$$\frac{\partial F_{0,1}}{\partial k_B} = \frac{1}{k_B}\sum_i\sum_j\sum_k \frac{\partial F_{0,1}}{\partial U_{ijk}}. \tag{12}$$

Finally, for the population we obtain

$$\frac{\partial\eta}{\partial p} = \phi(F_1 - F_0). \tag{13}$$

2.5. *Measurements*

The crystals were illuminated with a 0.2 W incident laser beam, which produced 0.1 W power in a 0.7 mm diameter area at the sample position. The performance of the instrumentation was checked by applying the modulation circuitry without laser illumination. The difference in normalized counts between the laser 'on' and 'off' counters for each step was found to be within the counting statistical error. The response ratio $\eta_I = (I_{on} - I_{off})/I_{off}$ converged to a nonsignificant value close to zero when measurements were continued for a sufficient length of time.

For the actual measurements, a single crystal of $[RhBr_2(py\text{-}d_5)]Br.6D_2O$ (py = pyridine; Fig. 3) with a 0.40 × 0.30 mm area and 0.08 mm thickness was used. To maximize heat dissipation, the crystal was mounted with its largest face parallel to the flat surface of a 4 mm diameter Al pin, the latter being in thermal contact with the heat reservoir of the cryostat. In this geometry the (100) direction of the crystal is almost aligned with the ϕ axis of the diffractometer. The structure of the complex at 40 K (Fig. 3) was determined in a separate experiment using imaging plates (Ozawa & Coppens, 1997). Cell dimensions are listed in Table 1. The linear absorption coefficient for 488 nm light was calculated as 5.888 mm^{-1}, using the absorbance of an aqueous solution of Rh complex at the same wavelength. Thomas, Watts & Crosby (1973) reported a measured lifetime τ_m of 2.440 ms for $[RhBr_2(py\text{-}d_5)]Br$ in D_2O–CH_3OD at 77 K and an intersystem crossing yield $\phi_{isc} = 1$. Assuming the same lifetime in the solid at 40 K,† we obtain, with expression (3), a 1.0% fractional population of the excited molecules in the crystal. Although the laser intensity can be increased by a factor of two, the small value demonstrates the limitation of the steady-state methods, such as employed in the current experiment. On the other hand, the modulation method employed is extremely sensitive and capable of detecting intensity differences of the order of a fraction of 1% (Graafsma, Coppens *et al.*, 1993).

To examine the relation between the modulation frequency and the rise in temperature, experiments were performed at the frequencies of 20, 40 and 80 Hz. Since, during each period, X-ray measurements are only started after a delay time δ (see Fig. 2) to allow for the rise to steady-state concentration, the effective measuring time per period equals $(1/2\nu) - \delta$. The delay time δ must be $> \tau$ to allow establishment of a steady-state concentration. With δ selected as 3 ms, use of the higher frequency of 80 Hz reduces measurement time by almost 50% and is therefore less efficient.

For each reflection the measurement was continued within the time limitations until the response ratio converged to a stable value. The convergence of the response ratios with time and intensity differences as a function of the scan angle ω are illustrated for the 008 reflection in Fig. 4. As in our previous electric-field experiments based on the modulation method, each reflection requires many hours of measurement time at the rotating-anode source. As a result, the total number of reflections measured in this study is limited. The ratio of the response ratio to its standard deviation is typically in the range 5–10, though larger (and smaller) values also occur (Table 3).

Table 1. *Crystallographic information and cell dimensions at 40 K*

a	12.510 (3) Å
b	10.570 (1) Å
c	21.402 (3) Å
β	98.31 (2)°
V	2800.3 Å^3
λ	0.7010 Å
μ	4.82 mm^{-1}
D_x	1.82 Mg m^{-3}
Space group	$P2_1/c$
Z	4

3. Results

3.1. *Wilson plots at different frequencies*

Wilson-type plots of $\ln(I_{on}/I_{off})$ against $2(\sin\theta/\lambda)^2$ for a number of reflections measured at chopper frequencies of 20, 40 and 80 Hz are shown in Figs. 5(*a*), 5(*b*) and 5(*c*), respectively. The temperature increase during the laser exposure is apparent from the slope of the least-squares line, which corresponds to ΔB, the change in the overall temperature factor B. The exposure time during each light-on period is reduced by increasing the frequency. If the temperature T increases linearly with laser exposure time, the average temperature increase $\langle\Delta T\rangle$ during each X-ray exposure period will be proportional to the average time $\langle t\rangle = [1/(2\nu) + \delta]/2$, where ν is the chopper frequency and δ the delay time. On the other hand, during the laser-off period, cooling is assumed to be rapid because of the lack of heat input during this part of the cycle and the specific mounting of the sample described above. The reduction in the temperature increase with increasing frequency is confirmed by the experiment, ΔB being reduced from

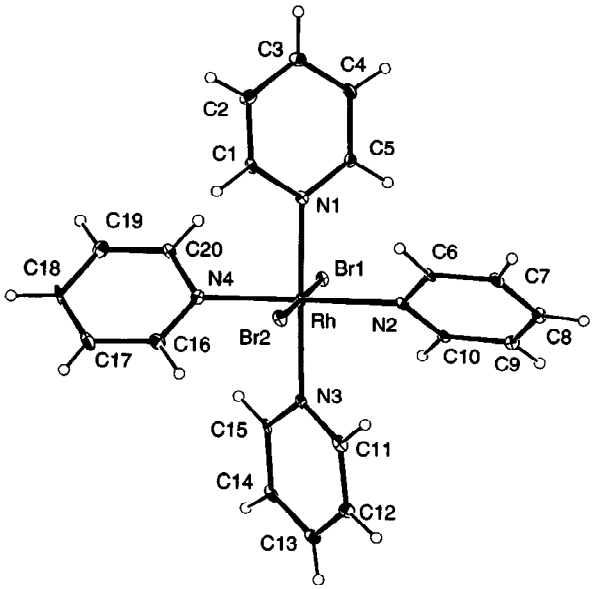

Fig. 3. *ORTEP* (Johnson, 1976) drawing of the ground-state structure at 40 K (Ozawa & Coppens, 1997).

† Our measurement on the crystal at 40 K gives a lifetime of the order of 1–2 ms.

Table 2. *Results of response ratio refinements*

In refinements 1 and 2 only the temperature scale factors are refined. In refinement 3, the y parameters of the Br atoms are included as variables; in refinement 4 the two Rh–Br bond lengths are constrained such that the shifts on molecular excitation are equal. The ground state y coordinates are as follows: Rh 0.27104 (3); Br1 0.50141 (3); Br2 0.03973 (3).

Refinement	No. of reflections	k_B (20 Hz)	k_B (40 Hz)	k_B (80 Hz)	y(Br1)	y(Br2)	$R(\eta)$	GOF
1	49	1.060 (4)	1.058 (3)	1.043 (6)			0.36	5.74
2	46	1.059 (3)	1.060 (2)	1.037 (4)			0.33	3.69
3	46	1.059 (3)	1.062 (2)	1.035 (4)	0.490 (9)	0.049 (5)	0.32	3.56
4	46	1.059 (3)	1.062 (2)	1.035 (4)	0.492 (3)	0.049 (3)	0.32	3.52

0.057 to 0.039 to 0.034 Å^2 at 20, 40 and 80 Hz, respectively. A plot of ΔB *versus* $\langle t \rangle$ is shown in Fig. 6. Extrapolation to infinite frequency ($\langle t \rangle = 0$), shows ΔB to have a frequency-independent component, which we interpret as the presence of a small fraction of excited molecules in the crystal corresponding to a static disorder.

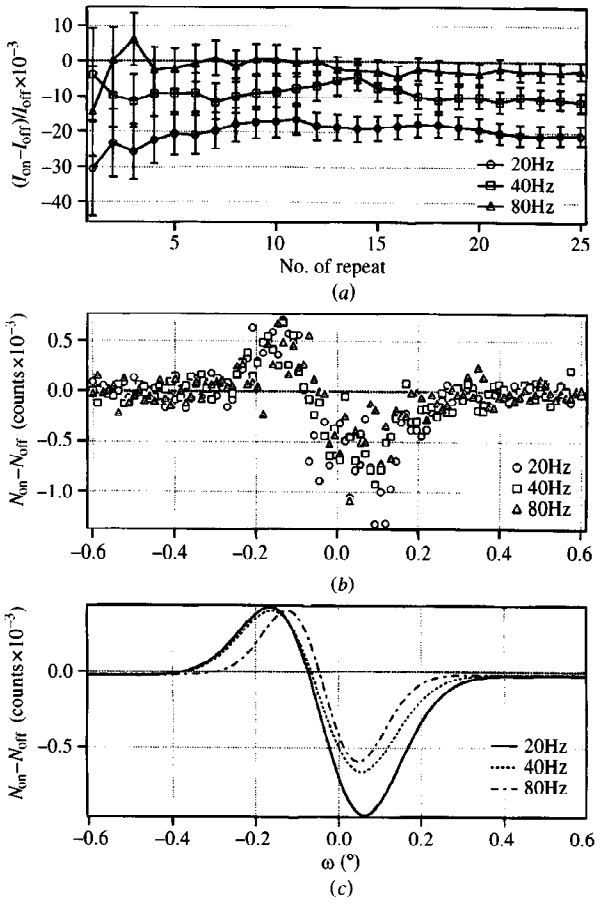

Fig. 4. Illustration of the response to laser irradiation, the 080 reflection ($\theta = 15.59°$) at different frequencies. (*a*) The convergence of the response ratio; (*b*) final values at each point of the step scan; (*c*) curves fitted to scans shown in (*b*), illustrating the peak shift upon irradiation and the dependence of the response ratio on frequency.

In contrast, a plot of the 4,0,18 response ratio (not shown here), measured at five different frequencies, extrapolates to a ΔB value close to zero. This result is

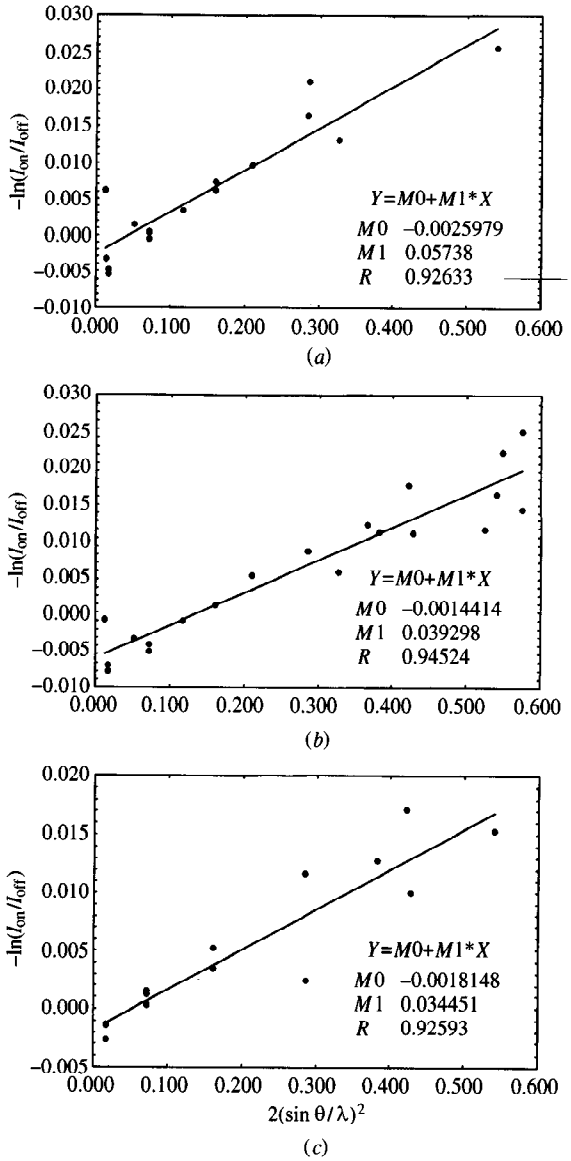

Fig. 5. Plots of $\ln\{I_{on}/I_{off}\}$ as a function of $2(\sin\theta/\lambda)^2$ for a number of different frequencies (*a*) 20 Hz, (*b*) 40 Hz and (*c*) 80 Hz.

Table 3. *Observed and calculated response ratios, refinement 3*

h	k	l	η	η_c	$\sigma(\eta)$	$\delta = \eta - \eta_c$	δ/σ
	20 Hz						
4	0	0	−0.00151	−0.00138	0.00035	−0.00013	0.36
6	0	0	−0.00341	−0.00256	0.00062	−0.00085	1.36
8	0	0	−0.00954	−0.00776	0.00061	−0.00178	2.93
10	0	0	−0.01295	−0.01426	0.00141	0.00132	0.93
0	2	0	0.00477	0.00038	0.00069	0.00440	6.39
0	4	0	−0.00033	−0.00158	0.00104	0.00125	1.21
0	8	0	−0.02084	−0.01318	0.00269	−0.00766	2.84
0	0	8	−0.00047	−0.00293	0.00050	0.00246	4.94
0	0	12	−0.00724	−0.00692	0.00083	−0.00032	0.38
0	0	8	0.00046	−0.00293	0.00052	0.00340	6.51
0	0	12	−0.00622	−0.00692	0.00086	0.00070	0.81
0	0	16	−0.01628	−0.01282	0.00161	−0.00346	2.15
0	0	22	−0.02535	−0.01681	0.00310	−0.00854	2.75
	40 Hz						
2	0	0	−0.00315	−0.00109	0.00023	−0.00206	8.82
4	0	0	−0.00091	−0.00146	0.00034	0.00055	1.61
6	0	0	−0.00303	−0.00271	0.00062	−0.00032	0.51
8	0	0	−0.00845	−0.00816	0.00060	−0.00029	0.48
10	0	0	−0.00877	−0.01499	0.00142	0.00622	4.39
0	2	0	0.00303	0.00035	0.00069	0.00268	3.89
0	4	0	0.00076	−0.00147	0.00101	0.00222	2.20
0	8	0	−0.01138	−0.01350	0.00274	0.00212	0.77
0	0	4	0.00227	−0.00060	0.00035	0.00287	8.26
0	0	8	−0.00010	−0.00309	0.00052	0.00299	5.69
0	0	12	−0.00490	−0.00728	0.00084	0.00238	2.85
0	0	16	−0.01135	−0.01347	0.00166	0.00212	1.28
0	0	22	−0.01819	−0.01767	0.00316	−0.00052	0.17
0	8	11	−0.01918	−0.01768	0.00178	−0.00151	0.85
2	9	−3	−0.01370	−0.00807	0.00140	−0.00563	4.01
3	9	5	−0.01343	−0.00789	0.00132	−0.00555	4.20
3	9	13	−0.01168	−0.01543	0.00210	0.00375	1.78
7	2	−20	−0.02300	−0.02004	0.00121	−0.00296	2.44
4	9	9	−0.01394	−0.01324	0.00147	−0.00070	0.47
1	11	5	−0.02546	−0.02271	0.00363	−0.00275	0.76
6	8	11	−0.01624	−0.02329	0.00357	0.00705	1.97
0	9	−2	−0.01454	−0.01190	0.00130	−0.00265	2.03
	80 Hz						
0	2	0	0.00268	0.00055	0.00070	0.00212	3.06
0	4	0	−0.00034	−0.00246	0.00103	0.00212	2.06
0	8	0	−0.00248	−0.01064	0.00262	0.00816	3.12
0	0	4	0.00138	−0.00028	0.00032	0.00166	5.20
0	0	8	−0.00120	−0.00167	0.00049	0.00047	0.95
0	0	12	−0.00348	−0.00403	0.00084	0.00056	0.66
0	0	4	0.00129	−0.00028	0.00035	0.00157	4.47
0	0	8	−0.00155	−0.00167	0.00053	0.00012	0.22
0	0	12	−0.00520	−0.00403	0.00086	−0.00117	1.36
0	0	16	−0.01154	−0.00760	0.00164	−0.00393	2.40
0	0	22	−0.01519	−0.00993	0.00320	−0.00526	1.64

in agreement with the main structural change on excitation being the variation of the axial Rh–Br bond lengths, which are oriented along the b axis. If this is the main distortion, the ($h0l$) reflections will be much less affected by the disorder.

3.2. *Least-squares refinements*

Results of a number of refinements are summarized in Table 2. To describe the ground state, parameters were taken from the low-temperature (40 K) structure determination (Ozawa & Coppens, 1997). All refinements were performed in two ways, with all 49 observations, and with only 46 observations, eliminating three response ratios in the 20 Hz data-sets which gave consistently poor fits even though, for the same reflections measured with different frequency, the fits were satisfactory. The refined temperature scale factors were found to be almost equal at 20 and 40 Hz, but lower at 80 Hz. The latter result is as expected, but the equality of the 20 and 40 Hz results is at variance with the ΔB values derived from the plots shown in Fig. 5, perhaps

as a result of the different weighting used in the two procedures. Assuming the B *versus* T dependence to be linear, the ΔB values correspond to temperature increases of 1.4–2.3 K.

Based on the spectroscopic results, the most important structural change is thought to affect the Rh–Br bonds (Thomas, Watts & Crosby, 1973). As they are aligned closely with the crystallographic y axis, the *h*0*l* reflections should be least affected, in agreement with frequency dependence of the response ratios for the 4,0,18 reflection, discussed above. In the second set of refinements the excited-state y coordinates of the Br atoms were allowed to vary. No significant correlation coefficients (> 0.5) between the three parameters were observed. It is encouraging that both Br atoms move in the same chemical direction, that is towards the Rh atom by similar amounts of, respectively, 0.12 (9) and 0.09 (5) Å. In a refinement in which both shifts are constrained to be equal, the reduction in the Rh–Br distance is 0.10 (4) Å, *i.e.* 2.5 times the estimated standard deviation. The shifts are not significant because of the limited size of the data-sets. Introduction of additional parameters such as the x and y coordinates of the Br atoms coordinated to Rh leads to unreasonably large shifts and removed any significant differences between the three temperature scale factors. Clearly, the size of the current data-set and the limited signal–noise ratio of the data do not allow the testing of more sophisticated models.

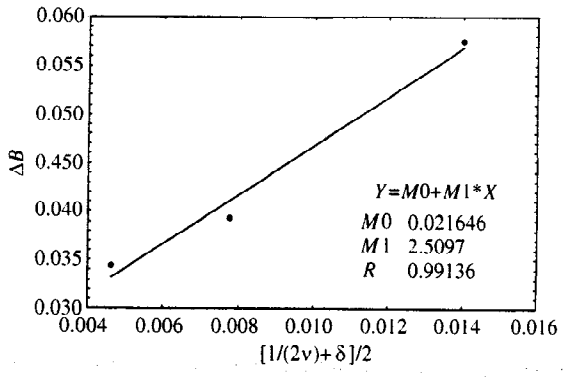

Fig. 6. Extrapolation of ΔB to infinite frequency.

4. Concluding remarks

The current work serves as a test of methods to be used in the study of light-excited crystals. Separation of the effects of the relatively small temperature increase and the geometric changes due to excitation is a prime requirement in such studies. The study presented here does not establish the geometry changes occurring on excitation of $[RhBr_2(py\text{-}d_5)]Br.6D_2O$, but shows how geometric and thermal effects can be separated and treated by established least-squares methods. Continuation of the studies requires larger data-sets which must be collected at high-intensity synchrotron sources.

We gratefully acknowledge the National Science Foundation (CHE9317770 and CHE9615586) and the Donors of The Petroleum Research Fund, administered by the American Chemical Society (PRF28664-AC3), for support of this research. YO is grateful to the Hyogo Prefecture Government, Japan, for financial support.

References

Carducci, M., Pressprich, M. R. & Coppens, P. (1997). *J. Am. Chem. Soc.* **119**, 2669–2678.

Coppens, P. (1997). *X-Ray Charge Densities and Chemical Bonding*. New York: Oxford University Press.

Coppens, P., Boehme, R., Price, P. F. & Stevens, E. D. (1981). *Acta Cryst.* A**37**, 857–863.

Fomitchev, D. V. & Coppens, P. (1996). *Inorg. Chem.* **35**, 7021–7026.

Graafsma, H., Coppens, P., Majewski, J. & Cahen, D. (1993). *J. Solid State Chem.* **105**, 520–527.

Graafsma, H., Paturle, A., Wu, L., Sheu, H.-S., Majewski, J., Poorthuis, G. & Coppens, P. (1992). *Acta Cryst.* A**48**, 113–120.

Johnson, C. K. (1976). *ORTEP II. Report ORNL-5138*. Oak Ridge National Laboratory, Oak Ridge, TN, USA.

Ozawa, Y. & Coppens, P. (1997). Unpublished results.

Paturle, A., Graafsma, H., Sheu, H.-S., Coppens, P. & Becker, P. (1991). *Phys. Rev.* B**43**, 683–691.

Pressprich, M. R., White, M. A., Vekhter, Y. & Coppens, P. (1994). *J. Am. Chem. Soc.* **116**, 5233–5238.

Restori, R. (1989). *ZACK Diffractometer Control Program*. SUNY at Buffalo Crystallography Software. SUNY, NY, USA.

Thomas, T. R., Watts, R. J. & Crosby, G. A. (1973). *J. Chem. Phys.* **59**, 2123–2131.